Nanosecond isomers and the evolution of collectivity in stable, even-math xmlns="http://www.w3.org/1998/Math/MathML">mrow>mi>A/mi>/mrow>/math> Hg isotopes

Saket Suman, S. K. Tandel, Ankit Kumawat, S. G. Wahid, M. Hemalatha, P. Chowdhury, R. V. F. Janssens, M. P. Carpenter, T. L. Khoo, F. G. Kondev, T. Lauritsen, C. J. Lister, D. Seweryniak, and S. Zhu

Phys. Rev. C **103**, 014319 — Published 25 January 2021

DOI: 10.1103/PhysRevC.103.014319

Nanosecond isomers and the evolution of collectivity in stable, even-A Hg isotopes

Saket Suman,[1] S.K. Tandel [a],[1,2] Ankit Kumawat,[1] S.G. Wahid,[1] M. Hemalatha,[3] P. Chowdhury,[2] R.V.F. Janssens,[4,5] M.P. Carpenter,[6] T.L. Khoo,[6] F.G. Kondev,[6] T. Lauritsen,[6] C.J. Lister,[2,6] D. Seweryniak,[6] and S. Zhu [b6]

[1] *School of Physical Sciences, UM-DAE Centre for Excellence in Basic Sciences, University of Mumbai, Mumbai 400098, India*

[2] *Department of Physics, University of Massachusetts Lowell, Lowell, Massachusetts 01854, USA*

[3] *Department of Physics, University of Mumbai, Mumbai 400098, India*

[4] *Department of Physics and Astronomy, University of North Carolina at Chapel Hill, Chapel Hill, North Carolina 27599, USA*

[5] *Triangle Universities Nuclear Laboratory, Duke University, Durham, North Carolina 27708, USA*

[6] *Argonne National Laboratory, Argonne, Illinois 60439, USA*

[a] Corresponding author: sujit.tandel@cbs.ac.in, sktandel@gmail.com

[b] Present address: National Nuclear Data Centre, Brookhaven National Laboratory, Upton, New York 11973-5000, USA

Abstract

Isomeric states and associated collective structures have been studied up to high spin in ^{198,200,202}Hg using multi-nucleon transfer reactions and the Gammasphere array. A coupled rotational band, with possible four-quasiparticle character, is established in ^{198}Hg. Sequences built on two-quasiparticle, positive- and negative-parity levels are assigned to ^{202}Hg. New isomers in ^{202}Hg with $I^{\pi} = 7^{-}$ and 9^{-}, and $T_{1/2} = 10.4(4)$ ns and 1.4(3) ns, respectively, have been identified. A half-life of 1.0(3) ns is established for the $I^{\pi} = 12^{+}$ state in ^{200}Hg. $B(E2)$ values deduced from isomeric transitions in Hg isotopes indicate that, while collectivity near the ground state gradually diminishes from $N = 112$ to $N = 124$, it is found to increase for the 12^{+} and 9^{-} states up to $N = 118$, followed by a reduction for higher neutron numbers. Calculations using the Ultimate Cranker code provide insight into the variation of deformation with spin and allow for an understanding of observed band crossings. The evolution of collectivity with spin, and along the isotopic chain, is described.

PACS numbers: 21.10.Re, 21.60.Ev, 23.20.Lv, 27.80.+w

I. INTRODUCTION

Nuclei in the $A{\approx}200$ region, just below doubly-magic ^{208}Pb, exhibit diverse structural phenomena. Isotopes with several valence nucleons show evidence for moderate deformation [1–3], however, the proximity to both neutron and proton shell closures leads to a substantial contribution of intrinsic degrees of freedom (*e.g.* particle-hole excitations) to the level structure [4–7]. Isotopes of Hg, where both proton and neutron shells are almost filled, are characterized by oblate deformation near their ground states. For the generation of excited states, rotation is the preferred mode for isotopes with $A{\leq}200$, though the magnitude of the deformation decreases with the increase in neutron number, and the onset of the N=126 shell closure. Rotation alignment frequencies at oblate deformation for low-Ω, high-j orbitals, such as $i_{13/2}$ neutrons and $h_{11/2}$ protons tend to be lower than the corresponding ones for high-Ω orbitals at prolate deformation [8]. These alignments are, therefore, observed in isotopes close to the line of stability.

The high-spin structure of proton-rich Hg isotopes ($A{\approx}190$) has been established rather well through their population in fusion-evaporation reactions [9, 10]. Isotopes along the line of stability can be accessed by inelastic excitation or nucleon transfer reactions. To populate excited states at high spin in such reactions, heavy projectiles with energies above the Coulomb barrier are typically required. On the other hand, the neutron-rich region can be reached through projectile fragmentation [11, 12]. Light, stable Hg isotopes, such as ^{196,198}Hg, have been studied with (α,xn) reactions, while an incomplete fusion reaction has been utilized in the case of ^{200}Hg [1, 2, 13–17]. Heavy, stable Hg isotopes; *e.g.*, ^{202,204}Hg, have been studied earlier using (n,γ) and (d,pn) reactions [18, 19]. In order to reach high spin, multi-nucleon transfer reactions are quite useful. These isotopes (*e.g.* ^{198,200}Hg) have sufficient deformation and this leads to collective rotational band structures that can be traced up to high spin [2, 15]. It is of particular interest to delineate the competition between collective and intrinsic excitation modes as a function of spin in these nuclei. This will enable a determination of the relative importance of these excitation mechanisms and to quantify their role in the generation of angular momentum at low and high spins.

II. EXPERIMENT AND DATA ANALYSIS

Excited states in Hg isotopes (A=192-202) were populated through multi-nucleon $(1p, xn)$ transfer reactions with a 1450-MeV ^{209}Bi beam incident on a thick, 50 mg/cm^2 ^{197}Au target. The ^{209}Bi beam, with a natural pulsing of 82.5 ns, was delivered by the ATLAS accelerator at Argonne National Laboratory. In another experiment, a 1430-MeV ^{207}Pb beam was incident on a similar, 50 mg/cm^2 thick ^{197}Au target and, as a result of multi-nucleon transfer reactions followed by subsequent neutron evaporation, a number of Hg isotopes (A=194-204) were populated.

The present work is focused on the structure of ^{198,200,202}Hg. When comparing the population of the ^{198,200,202}Hg nuclei in the two reactions, new information on ^{198,200}Hg was extracted primarily from the first experiment with the ^{209}Bi beam, whereas the data on ^{202}Hg were mainly obtained from the second measurement using the ^{207}Pb beam. The Gammasphere array [20, 21], comprising 100 Compton-suppressed, high-purity germanium detectors, was used to record three- or higher-fold γ-ray coincidence events.

The data were sorted into three- and four-dimensional symmetric γ-ray energy histograms and analyzed using the Radware suite of programs [22]. To isolate prompt coincidence events, γ rays detected within $\pm$40 ns of the incidence of the beam pulse on the target, were inspected. Most of the spectra with gates on two transitions were free of contaminant γ rays. In some cases, gates on three transitions proved useful for clarifying possible ambiguities.

Lifetimes of metastable states in the nanosecond (ns) region were determined using the centroid shift method [23]. For this purpose, histograms of the time difference (Δt) between γ rays feeding and deexciting a level of interest were created. For successive transitions in a cascade, where the intervening state is short lived ($T_{1/2} << 1$ ns), the time difference spectrum is observed to be centered around Δt=0 (characteristic of prompt γ rays). When the intervening state is metastable, the centroid of the time difference is shifted by a value equal to the mean life of the state. Since the time response of the Gammasphere detectors is dependent on the energy of the γ ray, a comparison is typically made between transitions of similar energy from prompt and metastable states. The background subtraction was performed by gating on multiple peak-free regions in close proximity to the γ rays below and above the level of interest in order to obtain the time difference characteristic of photopeak-photopeak coincidences only. The quoted errors in the lifetimes were ascertained by combining the systematic uncertainty arising from the discrete binning of the time parameter and the statistical uncertainties in the determination of the centroids of the prompt and delayed time distributions.

The method of Directional angular Correlations from Oriented nuclei (DCO) [24, 25] was used to determine the multipolarity of transitions of interest. For this purpose, an asymmetric energy-energy matrix was constructed with γ rays detected at $90° \pm 10°$ with respect to the beam direction on one axis, and those detected at $30°/150° \pm 10°$ on the other. The experimental DCO ratio $R_{DCO}(\gamma)$ of a γ ray is then determined as:

$$R_{DCO}(\gamma) = \frac{I_\gamma(30°/150°, 90°)}{I_\gamma(90°, 30°/150°)} \tag{1}$$

where $I_\gamma(\theta_1, \theta_2)$ is the intensity of the γ ray observed at angle θ_1, in coincidence with a transition observed at angle θ_2. Typical values of $R_{DCO}(\gamma)$ for $\Delta I = 1$, 2 γ rays are found to be 0.5 and 1.0 for those with dipole and quadrupole character, respectively, with gates on stretched quadrupole transitions. While the applicability of the DCO technique to inelastic and transfer reactions is limited in comparison to what can be achieved following fusion evaporation, its reliability in the present case was demonstrated from an analysis of transitions of known multipolarity, unless a long-lived state separates the observed γ rays.

III. RESULTS

A. ^{198}Hg

Excited levels in ^{198}Hg had been investigated in earlier studies using (α,xn) reactions, first using coaxial and planar Ge(Li) detectors [1], and later with two Ge(Li) detectors and a conversion electron spectrometer [15]. In the first instance, levels up to $I^\pi = 14^+$ were established [1]. In a later experiment, the level scheme was conclusively determined up to $I^\pi = 18^+$, with the 20^+ level being tentatively assigned. The time distribution of conversion electrons was recorded to determine half-lives of isomers [15]. A negative-parity sequence was extended up to $I^\pi = 11^-$ [1] and later up to $I^\pi = 17^-$ [15].

In the present work, the decay scheme of ^{198}Hg was extended up to $I^\pi = (20^+)$ in the positive-parity sequence (Band 2 in Fig. 1) and $I^\pi = (23^-)$ in the case of the negative-parity levels (Bands 4 and 5 in Fig. 1), with the inclusion of 11 new transitions (Figs. 2 and 3). It was established that the 1021-keV transition, which had previously been placed above the 18^+ level [15], was not coincident with the 777-keV γ ray deexciting this state; however, it is in coincidence with all γ rays below the 16^+ level leading to its present revised placement (Fig. 1). A new, 1275-keV γ ray is observed to be in coincidence with all transitions in Band 2 below the 18^+ level (Fig. 3). Although its DCO ratio could not be determined, it is tentatively assigned an $E2$ character since it is part of a cascade of $E2$ transitions with increasing energy, characteristic of a rotational band. The cumulative half-life of the 10^+ and 12^+ states in ^{198}Hg, both of which are isomeric, was determined to both be 3.1(3) ns through a centroid-shift analysis (Fig. 4), and found to be consistent with the previously reported values of 1.92(9) ns and 1.38(4) ns, respectively [26]. The relatively low energy (98 and 144 keV) and significant conversion coefficients for the $10^+ \rightarrow 8^+$ and $12^+ \rightarrow 10^+$ transitions, respectively, limited the number of counts in the associated time-difference spectra, rendering it unfeasible to separately infer the half-life of the 10^+ level.

Two rotational sequences with negative parity were identified above the (16^-) and 17^- levels and found to extend up to $I^\pi = (22^-)$ and (23^-), and $E_x \approx 6.4$ MeV (Bands 4 and 5 in Fig. 1). The 1021-keV and 1149-keV γ rays deexcite these sequences to the positive-parity band (Fig. 1). The 1149-keV γ ray is determined to be of dipole character, based on its DCO ratio (Table I). Further, the DCO ratio of the 334-keV transition, feeding the 15^- level, attests to its quadrupole character (Table I). With $M2$ character ruled out by the observed prompt decay of the $E_x = 4637$-keV level, the $E2$ assignment for the 334-keV transition, which was tentatively proposed in the previous work [15], is confirmed. This fixes the spin-parity of the 4637-keV level as $I^\pi = 17^-$, consistent with the dipole character for the 1149-keV γ ray. It may be noted that while the DCO ratios determined for most of the γ rays are consistent with the assigned multipole order, in the case of the 556- and 1021-keV transitions, the values do not clearly indicate either dipole or quadrupole character. The spin-parity assignment of $I^\pi = 11^-$ for the $E_x = 2468$-keV level is based on previously reported angular distribution measurements [1, 15] and the rotation-like character of Band 3. The $I^\pi = (16^-)$ assignment for the $E_x = 4509$-keV level follows from the spin-parity assignment of the 17^- level in Band 4, the observed coincidence relationships between Bands 4 and 5 and the corresponding excitation energies, and may therefore be considered tentative. The observation of weak, but distinct, coincidence relationships between transitions in Bands 4 and 5 (though the connecting, low-energy $\Delta I = 1$ transitions are not visible, possibly due to their large conversion coefficients) suggest that these two sequences constitute a coupled rotational band. These relationships are evident in Fig. 2 with coincidence gates placed on the 1149- and 1021-keV transitions. In addition to the transitions in Band 4 which are visible in a coincidence spectrum with a gate on the 1149-keV γ ray, a weak peak at 486 keV is also seen (Fig. 2). Similarly, with a gate on the 1021-keV γ ray, a weak peak at 570 keV is also observed (Fig. 2) in addition to the transitions in Band 5. This indicates the presence of unobserved, connecting $\Delta I = 1$ transitions between Bands 4 and 5. Additionally, the variation in energy of the levels in these sequences is typical of the small signature splitting observed in a coupled rotational band. Though there is no information on DCO ratios of transitions in Bands 4 and 5 (Fig. 1), based on the above observations and systematics in lighter, even-Hg isotopes [2, 15, 27] wherein similar band structures are observed, quadrupole character is most likely for γ rays in these sequences, but these assignments remain tentative as indicated in Fig. 1.

B. ^{200}Hg

The excited level structure of ^{200}Hg had been previously investigated using the incomplete fusion reaction ^{198}Pt(^{9}Be, $\alpha 3n$) [2]. The yrast, positive-parity structure was established up to the $I^{\pi} = 20^{+}$ state. The negative-parity band was identified up to the $I^{\pi} = (21^{-})$ level. The half-lives of the 7^{-} and 9^{-} states, populated in the β^{-} decay of ^{200}Au, had been previously established to be $\leq$0.8 ns and 1.07 ns, respectively [26].

The 10^{+} and 12^{+} states in the yrast structures of lighter, even-A Hg isotopes were established to have isomeric character from α-induced reactions on Pt targets [1, 13, 15]. To establish the half-life of the $I^{\pi} = 12^{+}$ state in ^{200}Hg, which had not been reported earlier, the difference in time of the γ rays feeding and deexciting this level (397 and 498 keV, respectively) was plotted and compared with that of prompt transitions of similar energy. A value of $T_{1/2} = 1.0(3)$ ns is established (Fig. 5a). For comparison, the half-life of the 12^{+} level in ^{190}Pt, also populated in this experiment, is determined to be 1.2(3) ns from the present work (Fig. 5b), consistent with the adopted value of 1.39(12) ns [14]. Unfortunately, it was not possible to determine the half-life of the $I^{\pi} = 10^{+}$ level, given the low γ-ray intensity of the feeding and deexciting transitions with energy 94 and 977 keV, respectively.

C. ^{202}Hg

The low-spin structure of ^{202}Hg had been determined in earlier studies using ^{201}Hg(n,γ) [18] and ^{202}Hg(d,pn) [19] reactions. Levels up to $I^{\pi} = 6^{+}$ and (5^{-}) and $E_x \approx 2.0$ MeV in the positive- and negative-parity sequences had been identified. In the present work, the level scheme is extended up to $E_x \approx 7.7$ MeV with the inclusion of fifteen new transitions (Fig. 6 and Table II). The half-lives of the (7^{-}) and (9^{-}) states in ^{202}Hg are newly determined. Values of $T_{1/2} = 10.4(4)$ ns and 1.4(3) ns for the (7^{-}) and (9^{-}) levels, respectively, are determined from centroid shift analyses (Fig. 7).

A newly identified sequence of transitions (Band 3) is established in coincidence with γ rays below the $I^{\pi} = 5^{-}$ level at $E_x = 1965$ keV (Fig. 6). Transitions with energy 94, 163, 598, 956, 379 and 338 keV are placed in cascade based on coincidence and intensity considerations (Figs. 8 and 9). The transitions observed in the delayed regime from the decay of the (7^{-}) isomer are displayed in Fig. 10. The spin-parity assignments for the associated levels are based on systematics of even-A Hg isotopes, *e.g.*, 5^{-} and (7^{-}) states with an energy spacing $\lessapprox$100 keV have been identified in $^{194-200}$Hg [28–31]. The assignment of spin-parity for the (7^{-}) and (9^{-}) levels follows similar considerations. Since unambiguous data on multipolarities are not available from the present experiment, the assignments should be viewed as tentative. The higher-lying transitions in Band 3 are placed according to their intensities. However, the corresponding levels are not assigned either spin or parity (Table II).

Band 1, which is built on the ground state, is identified up to the $I^{\pi} = 6^{+}$ level. The 163-keV γ ray in Band 3 and other transitions above it are observed to be in coincidence with the 440-, 680- and 869-keV members of Band 1 herewith implying the presence of an unobserved 71-keV transition linking the 6^{+} and (7^{-}) levels in the two bands. A second sequence of transitions (Band 2) with energies 220, 404, 730, 842, 629, 788 and 537 keV has been newly identified (Figs. 8 and 9). The relative placement of the 220-keV γ ray with respect to other transitions in Band 2 is based on the assumption of its $E2$ multipolarity. Band 2 is observed to feed the negative-parity Band 3 through the 693-keV transition. In neighboring, even-A Hg isotopes, positive-parity states with either $I^{\pi} = 10^{+}$ or 12^{+} are observed to deexcite to the negative-parity sequence. In view of the similarity of the decay pattern, the spin-parity of the 3513-keV state is tentatively assigned to be $I^{\pi} = (12^{+})$ since the deexciting transition feeds the (11^-) level. The levels above the $I^\pi = (12^+)$ level probably have positive parity similar to the structure of lighter even-A Hg isotopes, but firm experimental evidence is currently lacking and no spin-parity values are given in Fig. 6.

IV. DISCUSSION

A. Positive-parity states

Isotopes of Hg ($Z = 80$) with $A \geq 190$ are characterized by oblate ground state deformation [1, 2, 13, 15, 27]. The Total Energy Surface plot for the yrast, $I^\pi = 8^+$ state in ^{198}Hg (Fig. 11a), obtained using the Ultimate Cranker code [32] indicates a favored energy minimum for an oblate shape ($\epsilon_2 = 0.13$ and $\gamma = -66°$). At higher spin ($I^\pi = 16^+$), the oblate minimum is found to persist and move towards larger negative γ values (Fig. 11b), and eventually towards γ = -90°, indicating a triaxial, non-collective shape at the highest spins. The magnitude of deformation decreases gradually from A = 192 (N = 112) to A = 202 (N = 122) as the shell closure at N = 126 is approached. This is evident from the steady decrease in the reduced $E2$ transition probabilities [$B(E2)$] for $2^+ \rightarrow 0^+$ transitions with increasing neutron number in the even-mass isotopes (Figs. 12a and 12b). The $B(E2)$ values in Weisskopf units (W.u.) are obtained using the expression:

$$B(E2)(W.u.) = 9.52 \times 10^6 E_\gamma^{-5} A^{-4/3} [t^\gamma_{1/2}]^{-1} \tag{2}$$

where E_γ is the γ-ray energy in keV, A is the mass number of the nucleus, and $t^\gamma_{1/2}$ represents the partial half-life in seconds of the γ ray deexciting the level. Transition energies in the ground state band exhibit a regular increase up to the $I^\pi = 6^+$ level characteristic of a collective rotational behavior. The magnitude of $B(E2)$ values for the $2^+ \rightarrow 0^+$ transition ranges between 25 to 42 W.u. for A = 200-192, consistent with this interpretation (Table III).

A discontinuity in this regular ordering is visible beyond the 6^+ level and the 8^+, 10^+ and 12^+ states are found to be quite closely spaced in energy (Fig. 13), particularly for isotopes with A = 190-198, with the typical energy separation being $\lessapprox$ 100 keV. This rather abrupt discontinuity has been associated with the rotation-induced alignment of a pair of $i_{13/2}$ neutrons [15]. With a ground-state quadrupole deformation $\epsilon_2 = 0.13$, the cranking description of an oblate deformed rotor is more appropriate than the seniority scheme for spherical nuclei. A large increase in the moment of inertia is evident (Fig. 14a), and the resultant aligned angular momentum is deduced to be 12 $\hbar$ (Fig. 14b), consistent with the contribution from two $i_{13/2}$ neutrons. An alignment frequency of $\hbar\omega \approx 0.2$ MeV is evident. The neutron and proton quasiparticle energies in ^{198}Hg as a function of rotational frequency (Figs. 15a and 15b) have been calculated using the Ultimate Cranker code [32]. The first band crossing for $i_{13/2}$ neutrons (labeled AB in the standard convention [33]) is visible at $\hbar\omega$ = 0.19 MeV; in the case of $h_{11/2}$ protons, the corresponding crossing occurs at 0.31 MeV. Further, effective g-factors of -0.19(6) and -0.18(8) measured for the 10^+ and 12^+ states in ^{196}Hg and ^{198}Hg, respectively [34], clearly indicate a neutron configuration for the rotation-aligned band. The energies of the 10^+ and 12^+ states exhibit a marked increase from $N = 118$ to $N = 120$ (Fig. 13). This has been attributed to the filling of the $i_{13/2}$ subshell at $N = 120$ and the presence of a large energy gap beyond this neutron number [2]. The 12^+ states in even-mass Hg isotopes with A = 204, 206 lie at an even higher excitation energy. They are understood to arise from predominantly intrinsic excitations [35, 36] in contrast to the situation in the lighter isotopes where a collective nature is observed (Fig. 13 and Table III).

The variation of $B(E2)$ values with neutron number for the $2^+ \rightarrow 0^+$, $10^+ \rightarrow 8^+$ and $12^+ \rightarrow 10^+$ transitions is listed in Table III and illustrated in Fig. 12b. The $B(E2 : 2^+ \rightarrow 0^+)$ values are seen to decrease from 42 to 12 W.u. with the N = 112 to N = 124 change in neutron number. This is consistent with the reduction in collectivity expected when approaching the N = 126 shell gap. In contrast, the $B(E2 : 12^+ \rightarrow 10^+)$ and the $B(E2 : 10^+ \rightarrow 8^+)$ values exhibit an overall increasing trend from lighter to heavier isotopes. This increasing trend may be associated with the fact that orbitals with lower-Ω values in the $i_{13/2}$ subshell are occupied for larger neutron numbers, in contrast to higher-Ω ones for lighter isotopes. In the former instance, rotation-aligned coupling is favored as a result of which the enhancement in $E2$ transition rates is more pronounced [37], which in turn is reflected in higher $B(E2 : 12^+ \rightarrow 10^+)$ values.

Following the assignment of the 1275-keV, $(20^+) \rightarrow 18^+$ transition in ^{198}Hg from this work (Fig. 1), and the absence of any significant feeding from positive-parity levels above the 18^+ and (20^+) states, which could be associated with the continuation of the rotational sequence, it may be concluded that there does not appear to be any evidence for a CD neutron crossing. A similar situation was noted in the case of ^{200}Hg as well [2].

The 3513-keV level in ^{202}Hg, which is tentatively assigned $I^{\pi} = (12^{+})$, may be associated with the breaking of an $i_{13/2}$ neutron pair. This is supported by empirical calculations, using 1-quasiparticle energies from neighboring nuclei together with pair-gap energies calculated from odd-even mass differences and residual interactions deduced from isomeric states with the same configuration [7], which compute a $i_{13/2}$ broken-pair configuration at an excitation energy $E_x = 3554$ keV; only 41 keV higher than the $E_x = 3513$ keV experimental energy.

B. Negative-parity states

The negative-parity levels, specifically the $I^{\pi} = 5^{-}$, 7^{-} and 9^{-} states, are built on an AE configuration involving two neutrons, with one occupying the $i_{13/2}$ subshell, and the other a low-j orbital (either $p_{1/2}$, $p_{3/2}$ or $f_{5/2}$). The $7^{-} \rightarrow 5^{-}$ and $9^{-} \rightarrow 7^{-}$ transitions are isomeric, and are enhanced by an amount which is approximately similar to that observed for the $2^{+} \rightarrow 0^{+}$ ones (Fig. 12a and Table III). The contribution from neutrons to the configuration of these states, in contrast to those in Pt isotopes where protons are also involved [38, 39], is borne out by the measured g-factors of -0.030(17) and -0.033(14) for the 7^{-} states in ^{196}Hg and ^{198}Hg, respectively [34]. The clear variation in the excitation energies of the 7^{-} and 9^{-} states with the change in neutron number also attests to the underlying neutron configuration (Fig. 13). These levels are lowest in energy around $N = 118$ since, for this neutron number, both the high- and low-j orbitals involved are closest to the Fermi surface.

Negative-parity levels at high spin, beyond $I = 15\ \hbar$, in even-mass Hg isotopes from $A =$ 190-196 have been associated with an $i_{13/2}$, BC neutron crossing in the band built on the AE configuration, since the AB crossing is blocked [27, 40]. This assignment is consistent with an intensity flow that primarily proceeds within the negative-parity sequence (AE at low and $ABCE$ at high spin). In the band crossing region, only a small fraction of the intensity from the negative-parity sequence is observed to feed the positive-parity levels. Further, the calculated value of the BC crossing frequency is in agreement with that observed in experiment. The observations in ^{198}Hg are significantly different. The major portion of the decay from Bands 4 and 5 (Fig. 1) is observed to feed the positive-parity levels in Band 2 with only a small fraction to Band 3 with the AE configuration; this would be difficult to reconcile with a pure $ABCE$ assignment for Band 4. Further, if Band 4 were to be hypothetically considered to have only the above rotation-aligned configuration, the BC crossing frequency inferred from experiment (0.29 MeV) would be quite different from the predicted value of 0.23 MeV. In the lighter Hg isotopes, the experimentally inferred and calculated values of such a BC crossing frequency are quite similar ($\hbar\omega \approx 0.2$ MeV). Additionally, since Band 5 appears to be a signature partner of Band 4, based on the experimental considerations listed in the previous section, it would have to be associated with an $ABCF$ configuration. However, no sequence associated with a possible AF configuration has been identified from the present or previous work. The decay from a hypothetical $ABCF$ sequence would preferentially populate the AF sequence, unlike the deexcitation to the positive-parity Band 2 noted in the present work. In view of the above considerations, it may be appropriate to associate Bands 4 and 5 with a 4-quasiparticle configuration arising from the breaking of an $i_{13/2}$ neutron pair. The origin of this configuration would be primarily attributed to intrinsic excitations rather than to the rotation-induced alignment characteristic of a collective rotational sequence. The spin and parity of the bandhead $I^{\pi} = 16^{-}$ can be understood as resulting from the coupling of three $i_{13/2}$ neutrons to $33/2$ $\hbar$ with the remaining being provided by a negative-parity orbital; *e.g.* either the $p_{3/2}$ or $f_{5/2}$ one. This change towards intrinsic character for high-spin, negative-parity levels in ^{198}Hg, in comparison to the rotation-aligned one in lighter even-A Hg isotopes, may be attributed to the reduction in collectivity at high spin occurring with increasing neutron number and consequent decreased predilection towards rotation alignment.

In ^{200}Hg, although the high-spin portion of the negative-parity levels has been associated with an $ABCE$ configuration [2], closer inspection of the data reveals that the $(17^{-}) \rightarrow 16^{+}$ transition has an intensity which is almost an order of magnitude larger than that observed for the "in-sequence", $(17^{-}) \rightarrow 15^{-}$ γ ray. This would be unusual with a pure $ABCE$ assignment. Further, the observations in $^{190-196}$Hg [27, 40] suggest that, for an $ABCE$ assignment, the primary feeding is seen to occur within the negative-parity sequence. In addition, with a hypothetical $ABCE$ configuration, the BC crossing frequency would be 0.3 MeV; *i.e.*, significantly higher than the calculated value. However, unlike in the present work on ^{198}Hg, a signature partner sequence is not identified in ^{200}Hg, perhaps due to a limited experimental sensitivity. The precise nature of the high-spin, negative-parity levels in ^{200}Hg can be ascertained once such a signature partner sequence is identified or if its presence can be ruled out in future work.The consideration of reduced collectivity at high spin in ^{198,200}Hg and the consequent possible limited role of the BC crossing in the negative-parity sequence in contrast to lighter, even-A Hg isotopes is also reflected in the positive-parity levels, where the CD crossing is observed up to ^{196}Hg, but not in ^{198,200}Hg.

In ^{202}Hg, the negative-parity levels at low spin appear to be qualitatively similar to those seen in the lighter, even-A Hg isotopes. While it is probable that the higher-lying members of Band 3 in ^{202}Hg are also of negative parity, in the absence of sufficient experimental evidence, any conclusion would be speculative. Future work, with linear polarization data for the high-spin transitions, may allow for a firm parity assignment.

V. SUMMARY

The structure of ^{198,200,202}Hg has been studied up to high spin. The level schemes of ^{198,202}Hg are considerably extended and new isomeric states with I^{π} = (7^-) and (9^-), and $T_{1/2} = 10.4(4)$ ns and 1.4(3) ns, respectively, are identified in ^{202}Hg. The half-life of the 12^+ state in ^{200}Hg is established to be 1.0(3) ns. The magnitude of collectivity has been deduced from reduced $E2$ probabilities for the $2^+ \rightarrow 0^+$, $10^+ \rightarrow 8^+$, $12^+ \rightarrow 10^+$, $7^- \rightarrow 5^-$, and $9^- \rightarrow 7^-$ transitions, as well as from moments of inertia and other observables. $B(E2)$ values for two-quasiparticle, positive- and negative-parity states are found to exhibit a maximum at neutron number $N = 118$. A rotational band with a possible four-quasiparticle structure is identified in ^{198}Hg. The AB, $i_{13/2}$ neutron crossing frequency in even-A Hg isotopes with oblate deformation, calculated using the Ultimate Cranker code, is in agreement with that deduced from experiment. While the CD neutron crossing had been established in isotopes up to ^{196}Hg, it is found to be absent in ^{198,200}Hg. The nature of the band structures in the vicinity of the expected BC crossing in ^{198,200}Hg is quite different from that in lighter, even-mass isotopes. A complex interplay between collective and intrinsic modes of excitation is evident at intermediate and high spin across the Hg isotopic chain.

VI. ACKNOWLEDGMENTS

The authors would like to thank I. Ahmad, J.P. Greene, A.J. Knox, D. Peterson, U. Shirwadkar, X. Wang and C.M. Wilson for assistance during the experiment. S.S. acknowledges support from the DST-INSPIRE PhD Fellowship of the Department of Science and Technology, Government of India (Fellowship No. IF170965). S.K.T would like to acknowledge support from the University Grants Commission, India, under the Faculty Recharge Programme. S.G.W. acknowledges support from the DST-INSPIRE Ph.D. Fellowship of the Department of Science and Technology, Government of India (Fellowship No. IF150098). M.H. would like to acknowledge support from the University Grants Commission, India, under the Faculty Recharge Programme. This work is supported by the U.S. Department of Energy, Office of Science, Office of Nuclear Physics, under award numbers DE-FG02-94ER40848 and DE-FG02-94ER40834, DE-FG02-97ER41041 (UNC) and DE-FG02-97ER41033 (TUNL), and contract number DE-AC02-06CH11357. The research described here utilized resources of the ATLAS facility at ANL, which is a DOE Office of Science user facility.

---

[1] D. Proetel, R.M. Diamond, F.S. Stephens, Nucl. Phys. **A231**, 301 (1974).

[2] A. Gorgen, H. Hubel, D. Ward, S. Chmel, R.M. Clark, M. Cromaz, A.O. Macchiavelli, K. Vetter, Eur. Phys. J. A **6**, 141 (1999).

[3] D. Negi, S.K. Tandel, P. Chauhan, P. Chowdhury, R. V. F. Janssens, M. P. Carpenter, T. L. Khoo, F. G. Kondev, T. Lauritsen, C. J. Lister, D. Seweryniak, and S. Zhu, Phys. Rev. C **100**, 014329 (2019).

[4] M.J.A. de Voigt, J. Dudek, Z. Szymanski, Rev. Mod. Phys. **55**, 949 (1983).

[5] S. G. Wahid, S. K. Tandel, P. Chowdhury, R. V. F. Janssens, M. P. Carpenter, T. L. Khoo, F. G. Kondev, T. Lauritsen, C. J. Lister, D. Seweryniak, S. Zhu, Q. B. Chen, and J. Meng, Phys. Rev. C **100**, 014328 (2019).

[6] S. G. Wahid, S. K. Tandel, Saket Suman, M. Hemalatha, Anurag Patel, Poulomi Roy, A. Y. Deo, Pragati, P. C. Srivastava, Bharti Bhoy, S. S. Bhattacharjee, R. P. Singh, S. Muralithar, P. Chowdhury, R. V. F. Janssens, M. P. Carpenter, T. L. Khoo, F. G. Kondev, T. Lauritsen, C. J. Lister, D. Seweryniak, S. Zhu, S. Rai, and A. Sharma, Phys. Rev. C **102**, 024329 (2020).

[7] Poulomi Roy, S.K. Tandel, Saket Suman, P. Chowdhury, R.V.F. Janssens, M.P. Carpenter, T.L. Khoo, F.G. Kondev, T. Lauritsen, C.J. Lister, *et al*, Phys. Rev. C **100**, 024320 (2019).

[8] U. S. Tandel, S. K. Tandel, P. Chowdhury, D. Cline, C. Y. Wu, M. P. Carpenter, R. V. F. Janssens, T. L. Khoo, T. Lauritsen, C. J. Lister, D. Seweryniak, and S. Zhu, Phys. Rev. Lett. 101 (2008) 182503.

[9] A. N. Wilson, J. Timar, J. F. Sharpey-Schafer, B. Crowell, M. P. Carpenter, R. V. F. Janssens, D. J. Blumenthal, I. Ahmad, A. Astier, F. Azaiez, *et al*, Phys. Rev. C **54**, 559 (1996).

[10] P. Fallon, T. Lauritsen, I. Ahmad, M. P. Carpenter, B. Cederwall, R. M. Clark, B. Crowell, M. A. Deleplanque, R. M. Diamond, B. Gall, F. Hannachi, R. G. Henry, R. V. F. Janssens, T. L. Khoo, A. Korichi, I. Y. Lee, A. O. Macchiavelli, C. Schuck, and F. S. Stephens, Phys. Rev. C **51**, R1609 (1995).

[11] M. Caamano, P.M. Walker, P.H. Regan, M. Pfutzner, Zs. Podolyak, J. Gerl, M. Hellstrom, P. Mayet, M.N. Mineva, A. Aprahamian *et al*, Eur. Phys. J. A **23**, 201 (2005).

[12] S.J. Steer, Zs. Podolyak, S. Pietri, M. Gorska, H. Grawe, K.H. Maier, P.H. Regan, D. Rudolph, A.B. Garnsworthy, R. Hoischen *et al*, Phys. Rev. C **84**, 044313 (2011).

[13] H. Helppi, S.K. Saha, P.J. Daly, S.R. Faber, and T.L. Khoo, Phys. Rev. C **28**, 1382 (1983).

[14] http://www.nndc.bnl.gov/ensdf

[15] C. Günther, H. Hübel, A. Kleinrahm, D. Mertin, B. Richter, D. Schneider, R. Tischler, Phys. Rev. C **15**, 1298 (1977).

[16] S.W. Yates, J.C. Cunnane, R. Hochel, and P.J. Daly , Nucl. Phys. **A222**, 301 (1974).

[17] C. Bernards, S. Heinze, J. Jolie, C. Fransen, A. Linnemann, and D. Radeck, Phys. Rev. C. **79**, 054307 (2009).

[18] D. Breitig, R.F. Casten, W.R. Kane, G.W. Cole, and J.A. Cizewski, Phys. Rev. C **11**, 546 (1975).

[19] P. Schüler, J. Recht, H. Wilzek, K. Hardt, C. Günther, K.P. Blume, K. Euler, and V. Kölschbach, Z. Phys. A - Atoms and Nuclei **317**, 313 (1984).

[20] I-Yang Lee, Nucl. Phys. **A520**, c641 (1990).

[21] R.V.F. Janssens and F.S. Stephens, Nucl. Phys. News **6**, 9 (1996).

[22] D.C. Radford, Nucl. Inst. Meth. Phys. Res. A **361**, 297 (1995).

[23] H.J. Kim, W.T. Milner, Nucl. Inst. and Meth. **95**, 429 (1971).

[24] K.S. Krane, R.M. Steffen, and R.M. Wheeler, Nucl. Data Tables **11**, 351 (1973).

[25] A. Kramer-Flecken, T. Morek, R.M. Lieder, W. Gast, G. Hebbinghaus, H.M. Jager, and W. Urban, Nucl. Inst. Meth. Phys. Res. A **275**, 333 (1989).

[26] H. Ton, G.H. Dulfer, J. Brasz, R. Kroondijk, and J. Blok, Nucl. Phys. A**153**, 129-144, 1970.

[27] H. Hübel, A.P. Byrne, S. Ogaza, A.E. Stuchbery and G.D. Dracoulis, Nucl. Phys. **A453**, 316 (1986).

[28] Balraj Singh , Nucl. Data Sheets **107**, 1531 (2006).

[29] Huang Xiaolong , Nucl. Data Sheets **108**, 1093 (2007).

[30] Huang Xiaolong and Kang Mengxiao, Nucl. Data Sheets **133**, 221 (2016).

[31] F. G. Kondev, S. Lalkovski, Nucl. Data Sheets **108**, 1471 (2007).

[32] R. Bengtsson, S. Frauendorf, Nucl. Phys. **A327**, 139 (1979).

[33] R. Bengtsson, S. Frauendorf, F.-R. May, Atomic and Nuclear Data Tables **35**, 15 (1986).

[34] A.I. Levon, Yu.V. Nosenko, V.A. Onischuk, A.A. Schevchuk, and A.E. Stuchbery, Nucl. Phys. **A764**, 24 (2006).

[35] J. Wrzesinski *et al.*, Phys. Rev. C. **92**, 044327 (2015).

[36] B. Fornal *et al.*, Phys. Rev. Lett. **87**, 212501 (2001).

[37] M. Guttormsen, A. Von Grumbkow, Y.K. Agarwal, K.P. Blume, K. Hardt, H. Hubel, J. Recht, P. Schuler, H. Kluge, K. H. Maier, *et al*, Nucl. Phys. **A398**, 119 (1983).

[38] S.K. Tandel, S.G. Wahid, P. Chowdhury, R.V.F. Janssens, M.P. Carpenter, T.L. Khoo, F.G. Kondev, T. Lauritsen, C.J. Lister, D. Seweryniak, S.Zhu, Phys. Lett. B **750**, 225 (2015).

[39] S.G. Wahid, S.K. Tandel, P. Chowdhury, R.V.F. Janssens, M.P. Carpenter, T.L. Khoo, F.G. Kondev, T. Lauritsen, C.J. Lister, D. Seweryniak, and S.Zhu, Phys. Rev. C. **92**, 054323 (2015).

[40] D. Mehta, Y. K. Agarwal, K. P. Blume, S. Heppner, H. Hubel, R. M. Leider, W. Urban, Z. Phys. A **339**, 317 (1991).

[41] Coral M. Baglin, Nucl. Data Sheets **113**, 1871 (2012).

[42] S. Zhu and F. G. Kondev, Nucl. Data Sheets **109**, 699 (2008).

[43] C. J. Chiara and F. G. Kondev, Nucl. Data Sheets **111**, 141 (2010).

[44] A. Esmaylzadeh, L. M. Gerhard, V. Karayonchev, J.-M. Régis, J. Jolie, M. Bast, A. Blazhev, T. Braunroth, M. Dannhoff, F. Dunkel, *et al*, Phys. Rev. C. **98**, 014313 (2018).

[45] T. Kibedi, T.W. Burrows, M.B. Trzhaskovskaya, P.M. Davidson, C.W. Nestor, Jr., Nucl. Instr. and Meth. A 589, 202 (2008).

TABLE I: Energies and intensities of γ rays, and energies and spins of initial and final levels in ^{198}Hg. DCO ratios are presented where available. Uncertainties in transition energies are up to 0.5 keV. Statistical uncertainties on γ-ray intensities and DCO ratios are listed.

E_γ (keV)	E_i (keV)	$\rightarrow$	E_f (keV)	I_i^π	$\rightarrow$	I_f^π	I_γ	DCO ratio
(47.7)	1684	$\rightarrow$	1636	7^-	$\rightarrow$	5^-	–	
97.5	2436	$\rightarrow$	2338	10^+	$\rightarrow$	8^+	–	
143.5	2579	$\rightarrow$	2436	12^+	$\rightarrow$	10^+	9.5(2)	
227.5	1911	$\rightarrow$	1684	9^-	$\rightarrow$	7^-	29.0(1)	0.93(6)
298.8	4808	$\rightarrow$	4509	(18^-)	$\rightarrow$	(16^-)	2.0(1)	
333.5	4637	$\rightarrow$	4304	17^-	$\rightarrow$	15^-	2.2(1)	0.86(9)
348.1	2927	$\rightarrow$	2579	14^+	$\rightarrow$	12^+	20.2(4)	0.99(3)
367.1	5004	$\rightarrow$	4637	(19^-)	$\rightarrow$	17^-	3.2(2)	
372.5	4637	$\rightarrow$	4264	17^-	$\rightarrow$	18^+	1.5(1)	
411.8	412	$\rightarrow$	0	2^+	$\rightarrow$	0^+	–	0.90(3)
485.6	5293	$\rightarrow$	4808	(20^-)	$\rightarrow$	(18^-)	2.2(1)	
521.8	2338	$\rightarrow$	1816	8^+	$\rightarrow$	6^+	26.9(6)	
524.2	2436	$\rightarrow$	1911	10^+	$\rightarrow$	9^-	15.0(3)	

E_γ (keV)	E_i (keV)	$\rightarrow$	E_f (keV)	I_i^π	$\rightarrow$	I_f^π	I_γ	DCO ratio
543.6	4808	$\rightarrow$	4264	(18^-)	$\rightarrow$	18^+	1.2(1)	
556.3	2468	$\rightarrow$	1911	11^-	$\rightarrow$	9^-	8.6(2)	0.66(6)
560.2	3487	$\rightarrow$	2927	16^+	$\rightarrow$	14^+	18.4(4)	0.95(4)
569.5	5574	$\rightarrow$	5004	(21^-)	$\rightarrow$	(19^-)	3.0(2)	
587.4	1636	$\rightarrow$	1049	5^-	$\rightarrow$	4^+	53.2(1)	0.62(5)
636.8	1049	$\rightarrow$	412	4^+	$\rightarrow$	2^+	100.0(2)	0.93(4)
673.2	5966	$\rightarrow$	5293	(22^-)	$\rightarrow$	(20^-)	1.2(1)	
740.1	5004	$\rightarrow$	4264	(19^-)	$\rightarrow$	18^+	1.7(1)	
767.6	1816	$\rightarrow$	1049	6^+	$\rightarrow$	4^+	27.3(4)	0.88(6)
776.9	4264	$\rightarrow$	3487	18^+	$\rightarrow$	16^+	5.5(2)	0.92(9)
803.5	6377	$\rightarrow$	5574	(23^-)	$\rightarrow$	(21^-)	1.6(1)	
859.1	3327	$\rightarrow$	2468	13^-	$\rightarrow$	11^-	4.6(3)	0.85(11)
976.9	4304	$\rightarrow$	3327	15^-	$\rightarrow$	13^-	3.0(2)	0.82(10)
1021.4	4509	$\rightarrow$	3487	(16^-)	$\rightarrow$	16^+	2.2(2)	0.74(13)
1149.3	4637	$\rightarrow$	3487	17^-	$\rightarrow$	16^+	4.2(2)	0.49(9)
1275.4	5540	$\rightarrow$	4264	(20^+)	$\rightarrow$	18^+	1.0(1)	

TABLE II: Energies and intensities of γ rays, and energies and spins of initial and final levels in ^{202}Hg. Uncertainties in transition energies are up to 0.5 keV. Statistical uncertainties on γ-ray intensities are listed.

E_γ (keV)	E_i (keV)	$\rightarrow$	E_f (keV)	I_i^π	$\rightarrow$	I_f^π	I_γ
(70.6)	2059	$\rightarrow$	1988	(7^-)	$\rightarrow$	6^+	–
94.2	2059	$\rightarrow$	1965	(7^-)	$\rightarrow$	5^-	9.3(18)
129.8	1311	$\rightarrow$	1181	4^+	$\rightarrow$	2^+	5.3(8)
163.3	2222	$\rightarrow$	2059	(9^-)	$\rightarrow$	(7^-)	34.1(30)
220.0	5710	$\rightarrow$	5490	–	$\rightarrow$	–	13.2(20)
221.8	1181	$\rightarrow$	960	2^+	$\rightarrow$	2^+	15.7(13)
337.5	4493	$\rightarrow$	4156	–	$\rightarrow$	–	–
351.5	1311	$\rightarrow$	960	4^+	$\rightarrow$	2^+	38.2(20)
379.1	4156	$\rightarrow$	3777	–	$\rightarrow$	(13^-)	11.3(18)
404.3	3918	$\rightarrow$	3513	–	$\rightarrow$	(12^+)	29.7(31)
439.5	440	$\rightarrow$	0	2^+	$\rightarrow$	0^+	–
520.0	960	$\rightarrow$	440	2^+	$\rightarrow$	2^+	67.6(30)
536.6	7663	$\rightarrow$	7126	–	$\rightarrow$	–	–

E_γ (keV)	E_i (keV)	$\rightarrow$	E_f (keV)	I_i^π	$\rightarrow$	I_f^π	I_γ
598.1	2820	$\rightarrow$	2222	(11^-)	$\rightarrow$	(9^-)	59.1(48)
629.0	6339	$\rightarrow$	5710	–	$\rightarrow$	–	15.5(24)
653.8	1965	$\rightarrow$	1311	5^-	$\rightarrow$	4^+	100.0(11)
680.3	1120	$\rightarrow$	440	4^+	$\rightarrow$	2^+	25.3(6)
692.8	3513	$\rightarrow$	2820	(12^+)	$\rightarrow$	(11^-)	32.1(37)
729.7	4647	$\rightarrow$	3918	–	$\rightarrow$	–	19.7(29)
787.6	7126	$\rightarrow$	6339	–	$\rightarrow$	–	–
842.3	5490	$\rightarrow$	4647	–	$\rightarrow$	–	18.8(30)
845.1	1965	$\rightarrow$	1120	5^-	$\rightarrow$	4^+	–
868.6	1988	$\rightarrow$	1120	6^+	$\rightarrow$	4^+	–
871.6	1311	$\rightarrow$	440	4^+	$\rightarrow$	2^+	22.3(19)
956.1	3777	$\rightarrow$	2820	(13^-)	$\rightarrow$	(11^-)	15.0(27)
959.9	960	$\rightarrow$	0	2^+	$\rightarrow$	0^+	–

TABLE III: Reduced transition probabilities, $B(E2)$, for the decay of metastable states in even-A Hg isotopes. Adopted values of half-lives are quoted from the current ENSDF database and published work [28–31, 41–44]. Only $E2$ branches have been included and $B(E2)$ values are rounded off to the nearest integer. Calculated conversion coefficients from BRICC have been used [45]. Asterisks indicate half-lives which are newly measured in the present work.

Isotope	E_x (keV)	I^π	$T_{1/2}$ (ns)	E_γ (keV)	$T^\gamma_{1/2}$ (s)	$T^W_{1/2}$(s)	$B(E2)$ (W.u.)
^{192}Hg	422.79	2^+	0.0146(55)	422.8	1.52×10^{-11}	6.36×10^{-10}	42(26)
	1977.03	$(7)^-$	1.018(55)	133.1	5.44×10^{-9}	2.06×10^{-7}	38(3)
	2507.3	$(10)^+$	3.6(5)	60.1	3.28×10^{-7}	1.10×10^{-5}	33(6)
	2535.5	$(12)^+$	11.1(5)	28.4	2.44×10^{-5}	4.65×10^{-4}	19(1)
^{194}Hg	427.9	2^+	0.0146(28)	427.9	1.52×10^{-11}	5.91×10^{-10}	39(10)
	1909.95	7^-	3.75(11)	96.95	3.13×10^{-8}	9.90×10^{-7}	32(1)
	2142.9	9^-	0.302(9)	232.9	3.73×10^{-10}	1.24×10^{-8}	33(2)
	2423.2	(10^+)	2.9(5)	59.5	3.72×10^{-7}	1.14×10^{-5}	31(7)
	2475.1	(12^+)	8.1(5)	52.0	9.19×10^{-7}	2.23×10^{-5}	24(2)
^{196}Hg	425.98	2^+	0.0159(21)	425.9	1.65×10^{-11}	5.97×10^{-10}	36(6)
	1841.34	7^-	5.22(16)	84.3	6.55×10^{-8}	1.96×10^{-6}	30(1)
	2064.35	9^-	0.355(18)	223.0	4.51×10^{-10}	1.52×10^{-8}	34(2)

Isotope	E_x (keV)	I^π	$T_{1/2}$ (ns)	E_γ (keV)	$T^\gamma_{1/2}$ (s)	$T^W_{1/2}$(s)	$B(E2)$ (W.u.)
	2342.3	(10^+)	4.83(19)	79.5	7.74×10^{-8}	2.63×10^{-6}	34(2)
	2439.0	(12^+)	3.5(1)	96.7	2.59×10^{-8}	9.89×10^{-7}	38(2)
^{198}Hg	411.8	2^+	0.02315(28)	411.8	2.42×10^{-11}	6.97×10^{-10}	29(1)
	1683.38	7^-	6.9(2)	47.74	1.18×10^{-6}	3.33×10^{-5}	28(1)
	1910.8	9^-	0.28(5)	227.5	3.51×10^{-10}	1.35×10^{-8}	38(9)
	2434.9	10^+	1.92(9)	97.3	1.99×10^{-8}	9.46×10^{-7}	48(3)
	2578.1	12^+	1.38(4)	143.2	3.19×10^{-9}	1.37×10^{-7}	43(2)
^{200}Hg	367.943	2^+	0.0464(4)	367.9	4.92×10^{-11}	1.21×10^{-9}	25(1)
	1962.59	7^-	≤ 0.8	111.1	3.57×10^{-8}	4.80×10^{-7}	≥ 13
	2143.77	9^-	1.07(4)	181.2	1.66×10^{-9}	4.17×10^{-8}	25(1)
	3215.1	12^+	1.0(3)$*$	94.2	3.05×10^{-8}	1.10×10^{-6}	36(16)
^{202}Hg	439.512	2^+	0.02726(22)	439.5	2.83×10^{-11}	4.90×10^{-10}	17(1)
	2059.0	(7^-)	10.4(4)$*$	94.2	8.69×10^{-8}	1.08×10^{-6}	12(1)
	2222.3	(9^-)	1.4(3)$*$	163.3	2.51×10^{-9}	6.92×10^{-8}	28(8)
^{204}Hg	436.552	2^+	0.0403(3)	436.5	4.18×10^{-11}	5.00×10^{-10}	12(1)

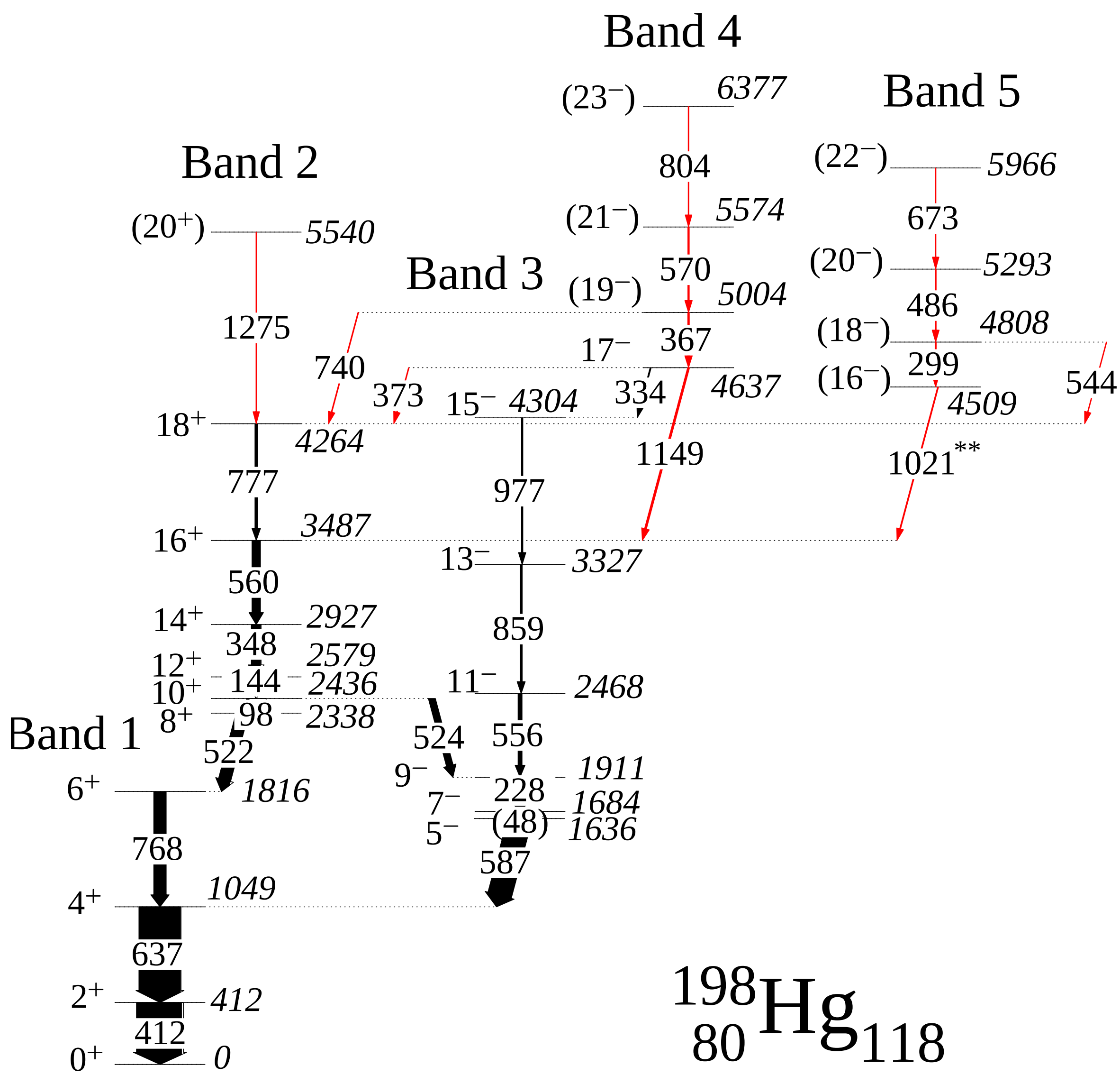

FIG. 1: Partial decay scheme of ^{198}Hg obtained from the present work. The transitions marked in red are the newly observed ones. The placement of the 1021-keV γ ray, marked with a double asterisk, is revised with respect to the previous work [15]. Bands 4 and 5 are newly established.

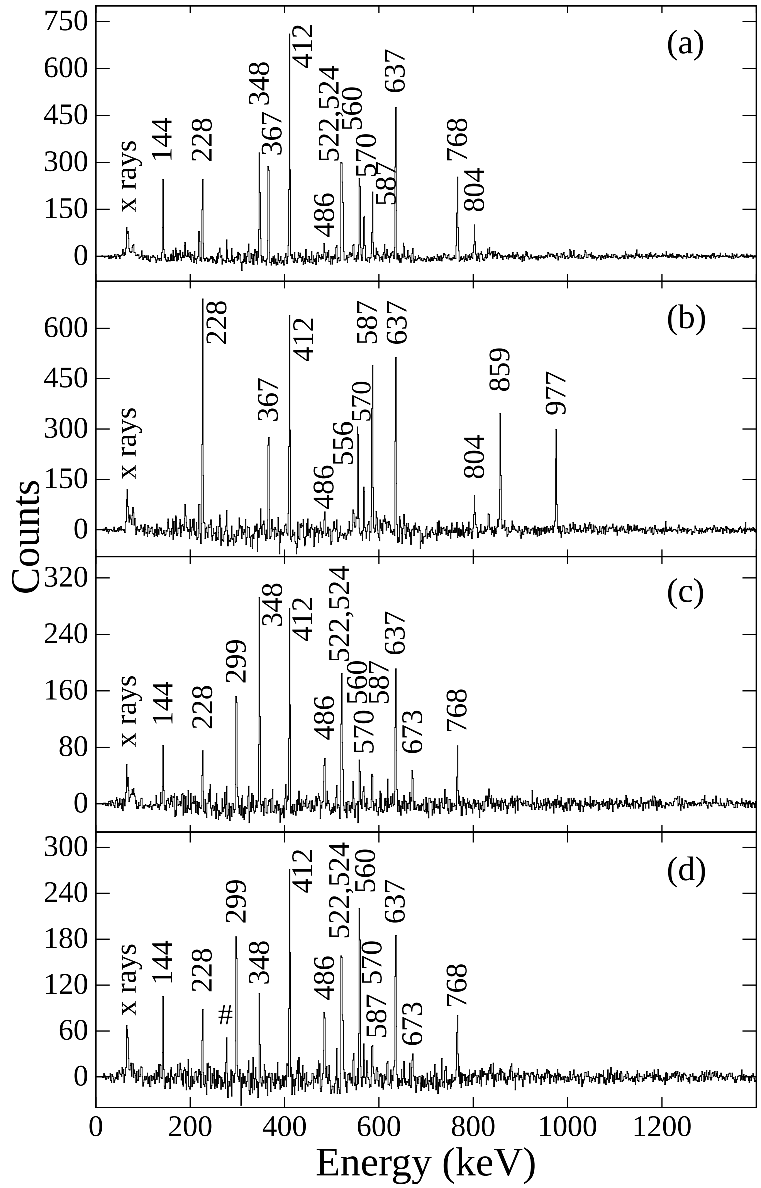

FIG. 2: Gated coincidence spectra displaying: (a), (b) Transitions above the $I^{\pi} = 17^{-}$ level in ^{198}Hg; note the 367-, 570- and 804-keV γ rays, and (c), (d) Transitions above the $I^{\pi} = 16^{-}$ state in ^{198}Hg; the 299-, 486- and 673-keV γ rays may be noted. The gating transitions are as follows: (a) 348 and 560 with 1149 keV (b) 556, 859 and 977 with 334 keV (c) 560 and 768 with 1021 keV, and (d) 348 and 768 with 1021 keV.

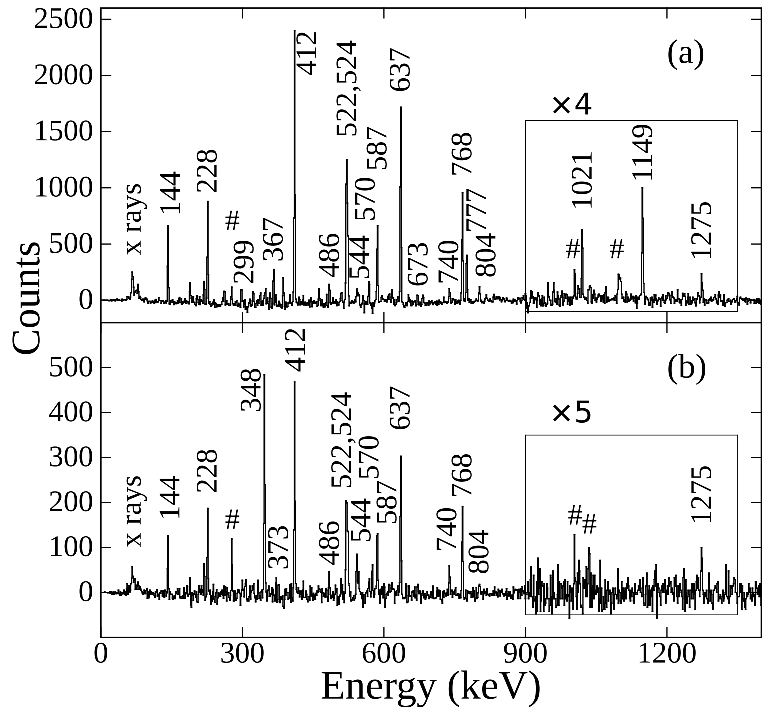

FIG. 3: Gated coincidence spectra for ^{198}Hg illustrating γ rays: (a) above the $I^{\pi} = 16^{+}$ level, which are coincident with the 348- and 560-keV transitions; (b) above the $I^{\pi} = 18^{+}$ level, which are coincident with the 560- and 777-keV transitions. The absence of the 1021-keV γ ray in the latter is consistent with its revised placement. The region above 1 MeV is enlarged for better visibility. The indicated contaminant transitions are present due to cross-coincidence with γ rays from ^{204,205}Pb isotopes which are binary partners of ^{198}Hg in multi-nucleon transfer followed by neutron evaporation, and from the Coulomb excitation of the target, ^{197}Au.

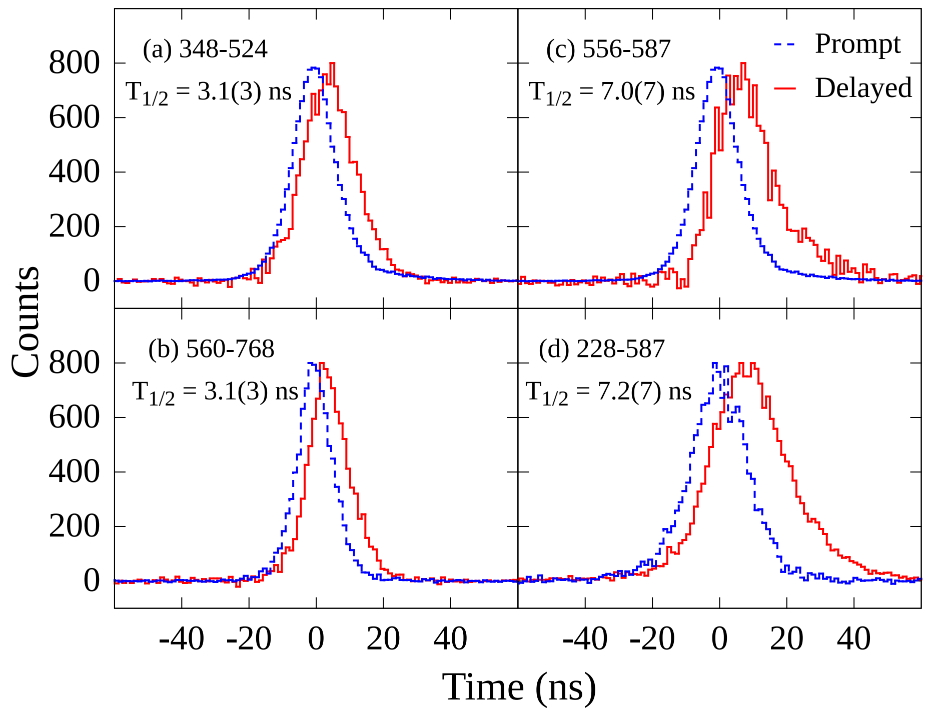

FIG. 4: Histograms of time difference between γ rays illustrating: (a), (b) the cumulative half-life of the 10^+ and 12^+ levels, both of which are isomeric, and (c), (d) the half-life of the 7^- state in ^{198}Hg. The dashed line displays the time difference between two transitions with similar energies which are prompt with respect to each other.

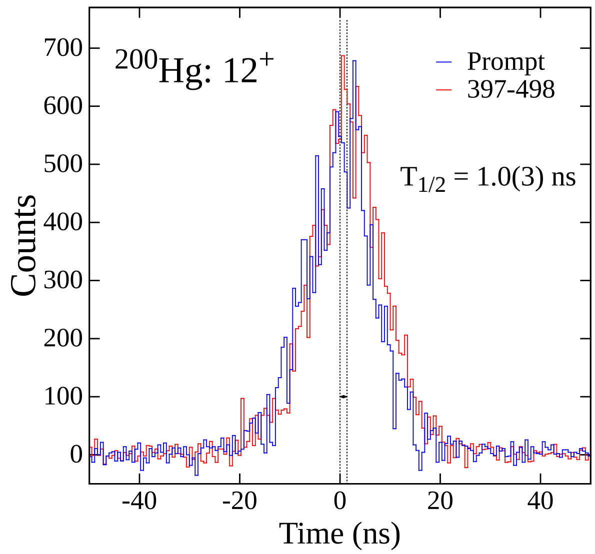

(a)

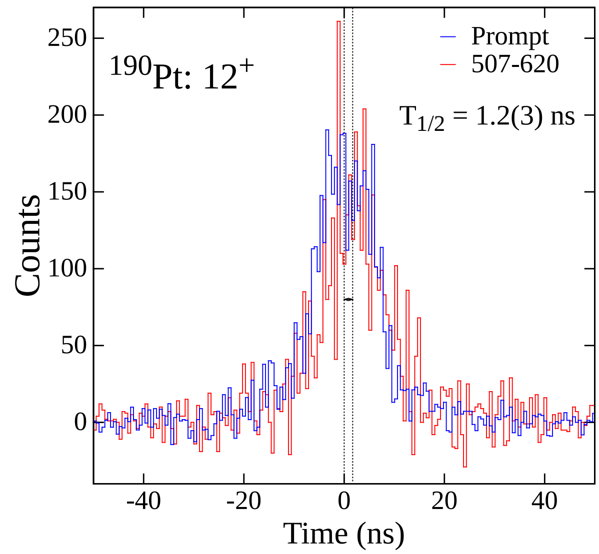

(b)

FIG. 5: Time difference spectra illustrating the determination of the half-life of the (a) 12^+ state in ^{200}Hg, (b) 12^+ state in ^{190}Pt, similar to that in Fig. 4. A value of $T_{1/2} = 1.0(3)$ ns is inferred for the 12^+ state in ^{200}Hg from the time difference between the 397- and 498-keV γ rays above and below the 12^+ level. In the case of ^{190}Pt, the inferred value of $T_{1/2} = 1.2(3)$ ns is consistent with the adopted value of 1.39(12) ns [14].

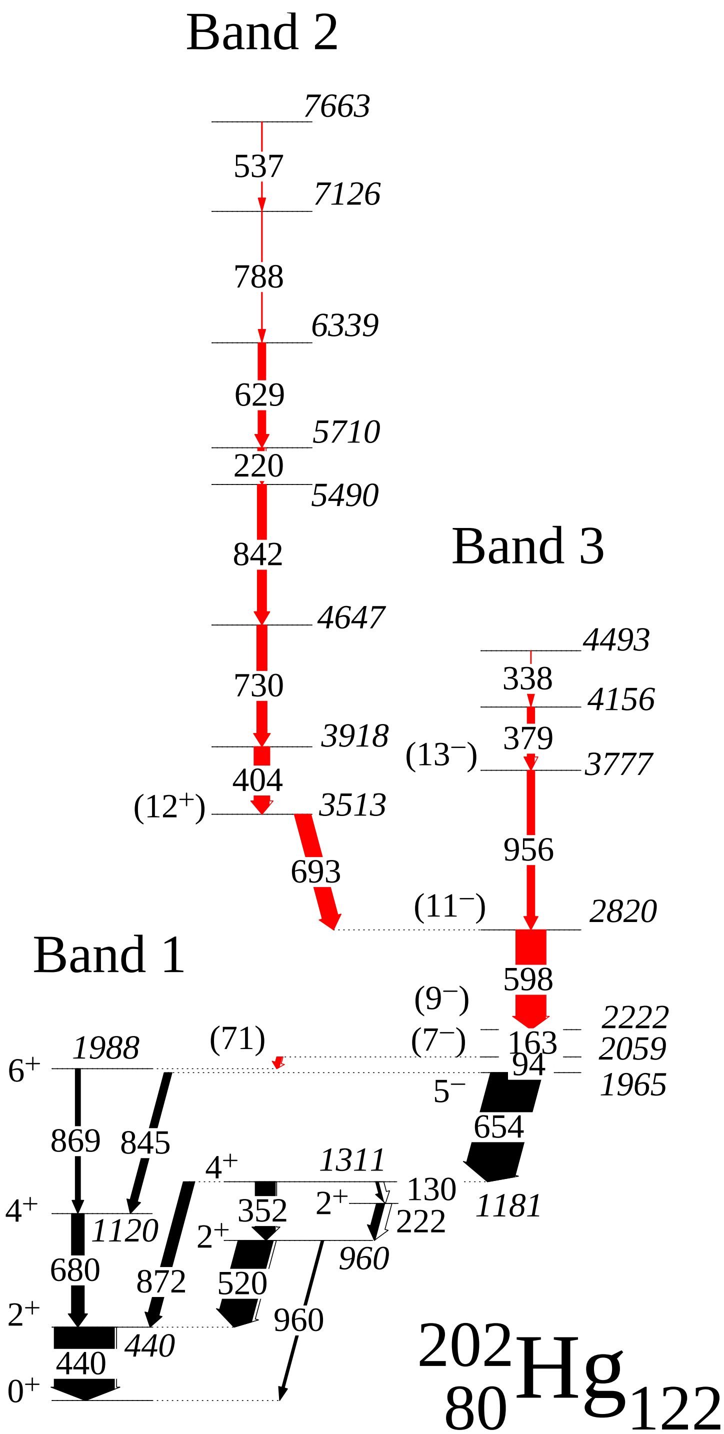

FIG. 6: Partial decay scheme of ^{202}Hg. The transitions marked in red are newly identified.

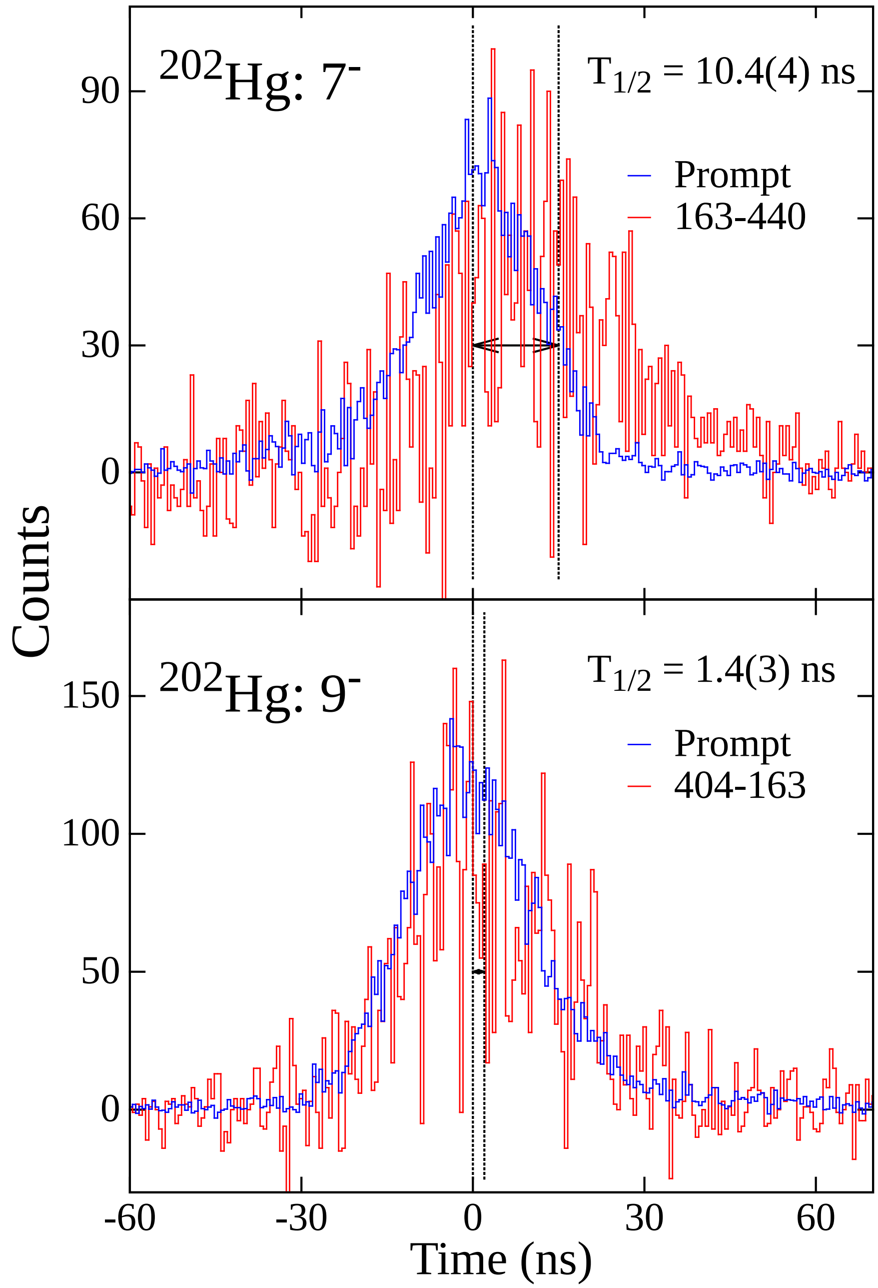

FIG. 7: Half-lives of the 7^- and 9^- states in ^{202}Hg determined using the centroid-shift method in a manner similar to Fig. 4.

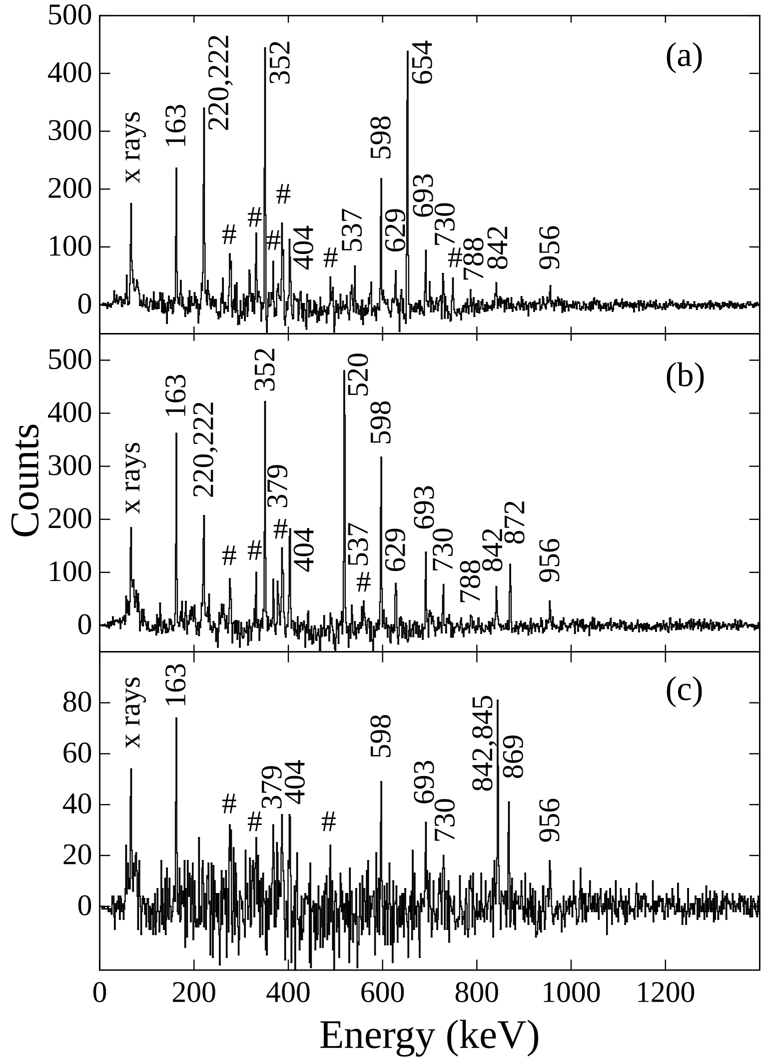

FIG. 8: Gated coincidence spectra from a prompt-coincidence cube (±30 ns) illustrating transitions in ^{202}Hg placed above the 7^- state in coincidence with the: (a) 440-520 (b) 440-654, and (c) 440-680 keV double gates. Contaminant peaks, originating from the presence of transitions with similar energy as the gating ones, in neighboring isotopes of Au, Hg and Tl (^{197}Au, ^{199,200}Hg and ^{200,201}Tl in Figs. 8 and 9), also populated in the reaction, are indicated with hash marks.

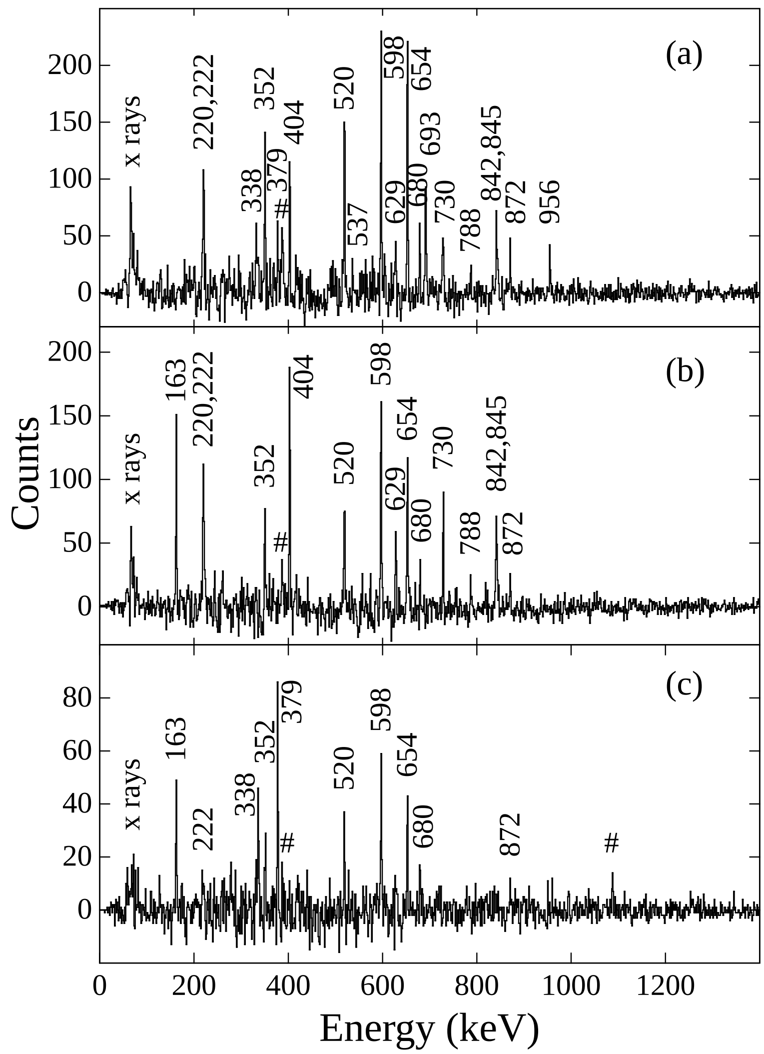

FIG. 9: Gated coincidence spectra from a prompt-coincidence cube (±30 ns) illustrating the branching above the 11^- level into Bands 2 and 3 in ^{202}Hg. In the (a) 163-440 keV double gate, coincidences with both bands are evident. In the (b) 440-693 keV double gate, only the transitions in Band 2 are visible. In the (c) 440-956 keV double gate, only the γ rays belonging to Band 3 are visible. Contaminant transitions (see caption of Fig. 8) are indicated with hash marks.

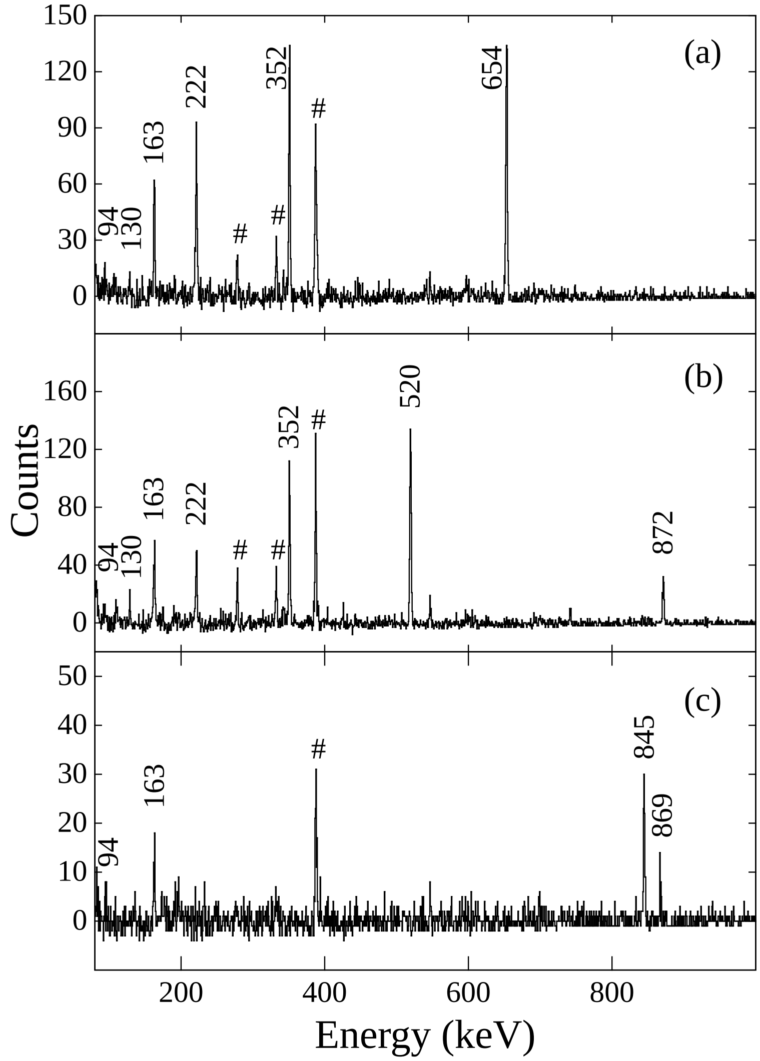

FIG. 10: Gated coincidence spectra from a delayed cube (>30 ns) displaying transitions in ^{202}Hg following the decay of the 7^- isomeric state in coincidence with: (a) 440-520 (b) 440-654, and (c) 440-680 keV double gates. Note the absence of prompt transitions present in Fig. 8. Contaminant transitions, from known long-lived activity, are indicated with hash marks.

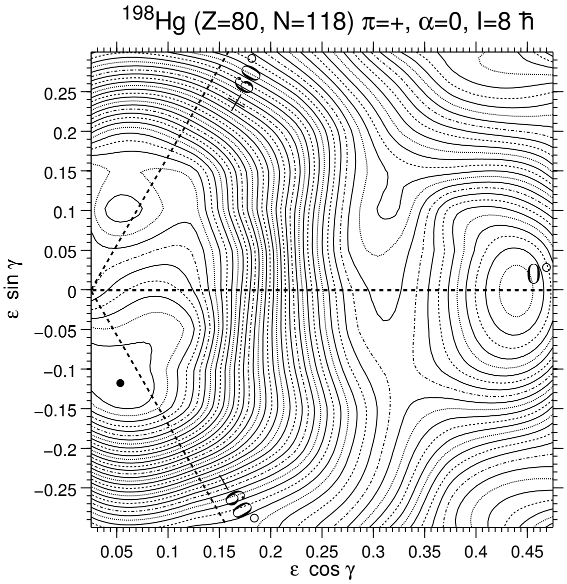

(a)

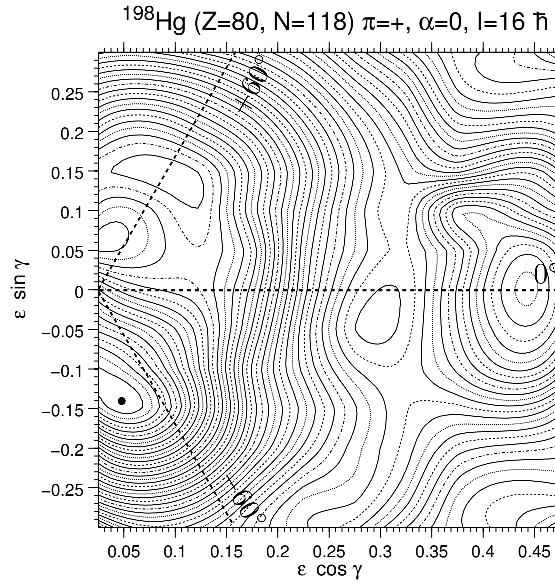

(b)

FIG. 11: Total energy surface plots illustrating energy minima in the positive-parity, yrast structure in ^{198}Hg obtained using the Ultimate Cranker code [32]. It is evident that (a) the lowest energy minimum is at $\epsilon_2 = 0.13$ and $\gamma = -66°$ for $I = 8\ \hbar$, and (b) at $\epsilon_2 = 0.15$ and $\gamma = -72°$ for $I = 16\ \hbar$.

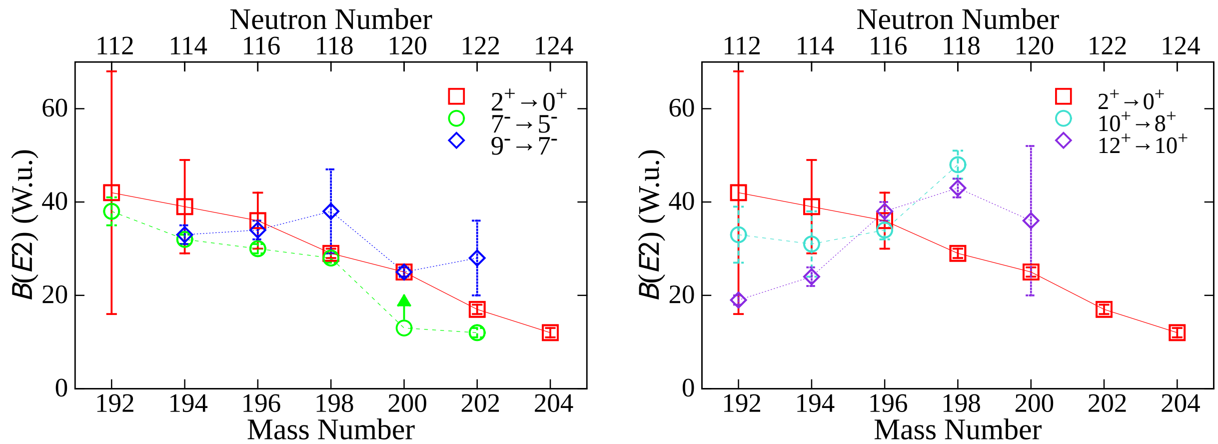

(a) (b)

FIG. 12: Reduced $E2$ transition probabilities in Hg isotopes (A = 192-204) for the: (a) 7^- $\rightarrow 5^-$ and $9^- \rightarrow 7^-$ isomeric transitions, and (b) $10^+ \rightarrow 8^+$ and $12^+ \rightarrow 10^+$ isomeric ones contrasted with the corresponding $2^+ \rightarrow 0^+$ values. The lines are intended to guide the eye. Details are provided in Table III and the text.

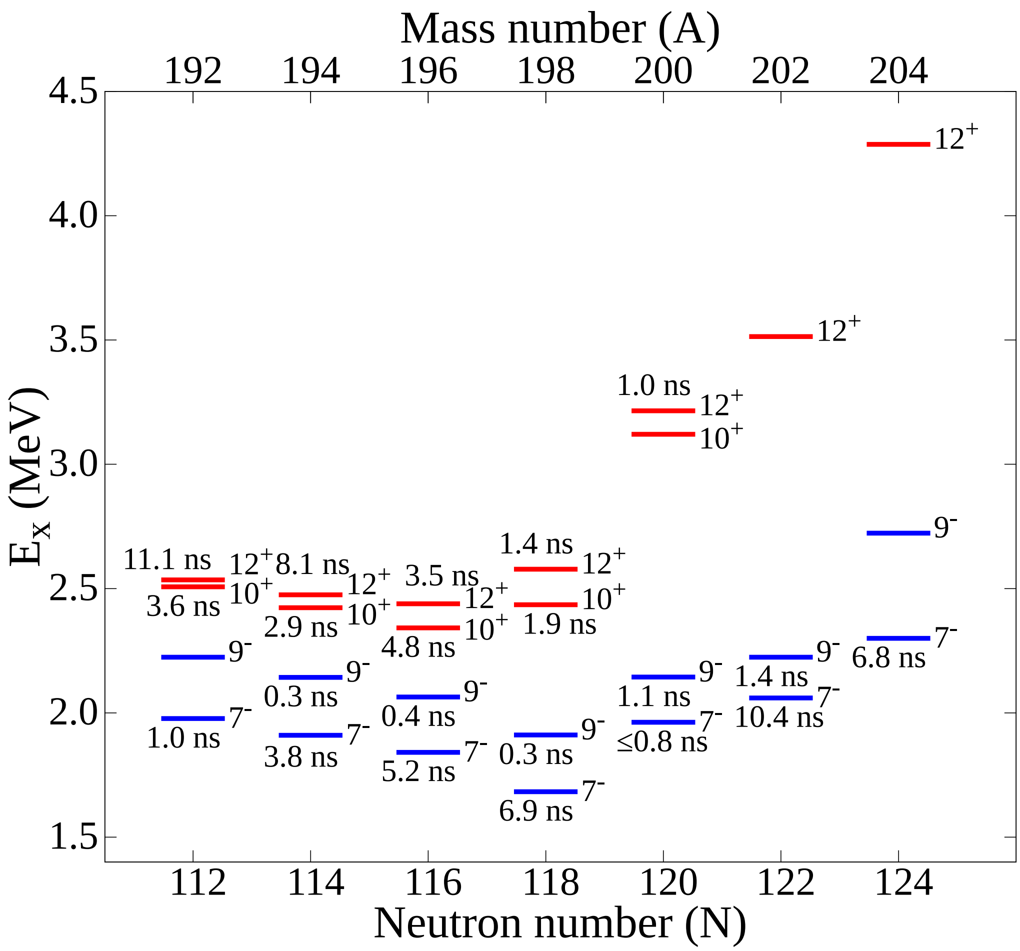

FIG. 13: Systematics of even-A Hg isotopes depicting the evolution in excitation energies and half-lives for the 7^-, 9^-, 10^+ and 12^+ states for A = 192-204.

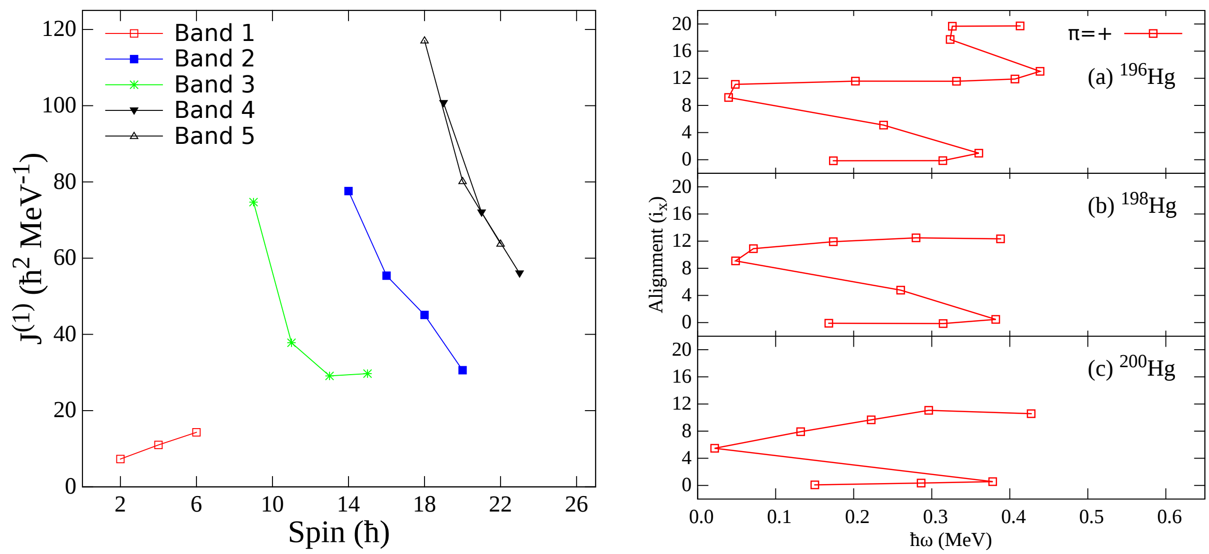

(a) (b)

FIG. 14: (a) Kinematic moment of inertia $\mathcal{J}^{(1)}$ as a function of spin for the bands in ^{198}Hg. (b) Aligned angular momentum as a function of rotational frequency for the yrast, positive-parity bands in ^{196,198,200}Hg. A reference rotor with $J_0 = 8\ \hbar^2$ MeV^{-1} and $J_1 = 35\ \hbar^4$ MeV^{-3}, appropriate for a comparison of the three isotopes, is used. Details are in the text.

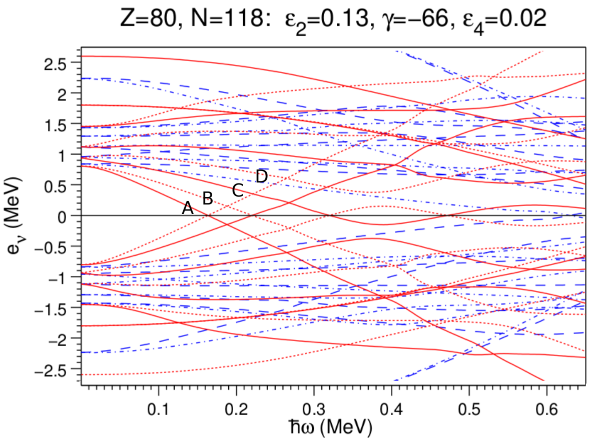

(a)

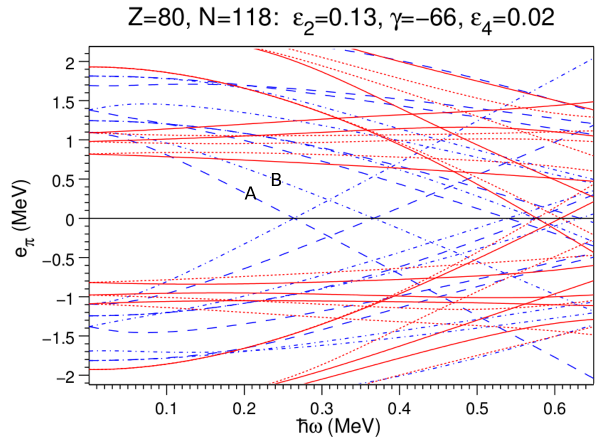

(b)

FIG. 15: (a) Neutron and (b) Proton quasiparticle energy levels for oblate deformation ($\epsilon_2 = 0.13$ and $\gamma = -66°$) in ^{198}Hg as a function of rotational frequency calculated using the Ultimate Cranker code [32]. The following (standard) convention is used for labeling the orbitals (lines) with different parity (π) and signature (α): (π, α) = (+, +1/2) [solid]; (π, α) = (+, -1/2) [short-dashed]; (π, α) = (-, +1/2) [dot-dashed]; (π, α) = (-, -1/2) [long-dashed].